Strain, Young’s modulus, and structural transition of EuTiO<inf>3</inf> thin films probed by micro-mechanical methods

Citation for the original published paper (version of record):
Manca, N., Tarsi, G., Kalaboukhov, A. et al (2023). Strain, Young’s modulus, and structural transition of EuTiO<inf>3</inf> thin films probed by micro-mechanical methods. APL Materials, 11(10). http://dx.doi.org/10.1063/5.0166762

APL Materials

RESEARCH ARTICLE | OCTOBER 06 2023

Strain, Young's modulus, and structural transition of $EuTiO_3$ thin films probed by micro-mechanical methods

Nicola Manca ✉ ; Gaia Tarsi ; Alexei Kalaboukhov ; Francesco Bisio ; Federico Caglieris ;
Floriana Lombardi ; Daniele Marré ; Luca Pellegrino

Check for updates

APL Mater. 11, 101107 (2023)
https://doi.org/10.1063/5.0166762

View Online
Export Citation
CrossMark

30 October 2023 07:31:09

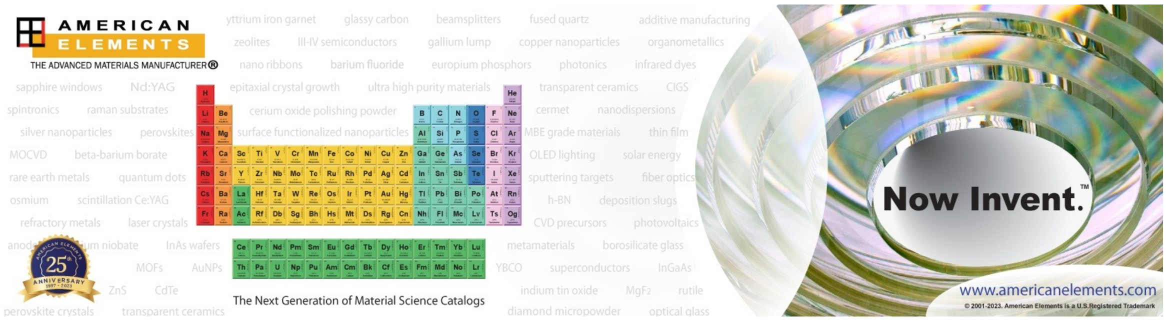

AMERICAN ELEMENTS
THE ADVANCED MATERIALS MANUFACTURER®
yttrium iron garnet glassy carbon beamsplitters fused quartz additive manufacturing
zeolites III-IV semiconductors gallium lump copper nanoparticles organometallics
nano ribbons barium fluoride europium phosphors photonics infrared dyes
sapphire windows Nd:YAG epitaxial crystal growth ultra high purity materials transparent ceramics CIGS
spintronics raman substrates cerium oxide polishing powder cermet nanodispersions
silver nanoparticles perovskites surface functionalized nanoparticles MBE grade materials thin film
MOCVD beta-barium borate OLED lighting solar energy
rare earth metals quantum dots sputtering targets fiber optics
osmium scintillation Ce:YAG h-BN deposition slugs
refractory metals laser crystals CVD precursors photovoltaics
InAs wafers metamaterials borosilicate glass
MOFs AuNPs YBCO superconductors InGaAs
ZnS CdTe indium tin oxide MgF2 rutile
perovskite crystals transparent ceramics diamond micropowder optical glass
The Next Generation of Material Science Catalogs
Now Invent.™
www.americanelements.com
© 2001-2023. American Elements is a U.S. Registered Trademark

AIP Publishing

APL Materials ARTICLE pubs.aip.org/aip/apm

Strain, Young's modulus, and structural transition of $EuTiO_3$ thin films probed by micro-mechanical methods

Cite as: APL Mater. 11, 101107 (2023); doi: 10.1063/5.0166762
Submitted: 7 July 2023 • Accepted: 18 September 2023 •
Published Online: 6 October 2023

View Online Export Citation CrossMark

Nicola Manca,[1,a)] Gaia Tarsi,[2] Alexei Kalaboukhov,[3] Francesco Bisio,[1] Federico Caglieris,[1] Floriana Lombardi,[3] Daniele Marré,[1,2] and Luca Pellegrino[1]

AFFILIATIONS

[1] CNR-SPIN, C.so F.M. Perrone, 24, 16152 Genova, Italy
[2] Dipartimento di Fisica, Università degli Studi di Genova, 16146 Genova, Italy
[3] Department of Microtechnology and Nanoscience - MC2, Chalmers University of Technology, SE 412 96 Gothenburg, Sweden

[a)] **Author to whom correspondence should be addressed:** nicola.manca@spin.cnr.it

ABSTRACT

$EuTiO_3$ (ETO) is a well-known complex oxide mainly investigated for its magnetic properties and its incipient ferro-electricity. In this work, we demonstrate the realization of suspended micro-mechanical structures, such as cantilevers and micro-bridges, from 100 nm-thick single-crystal epitaxial ETO films deposited on top of $SrTiO_3$(100) substrates. By combining profile analysis and resonance frequency measurements of these devices, we obtain the Young's modulus, strain, and strain gradients of the ETO thin films. Moreover, we investigate the ETO anti-ferro-distortive transition by temperature-dependent characterizations, which show a non-monotonic and hysteretic mechanical response. The comparison between experimental and literature data allows us to weight the contribution from thermal expansion and softening to the tuning slope, while a full understanding of the origin of such a wide hysteresis is still missing. We also discuss the influence of oxygen vacancies on the reported mechanical properties by comparing stoichiometric and oxygen-deficient samples.

INTRODUCTION

$EuTiO_3$ (ETO) is a complex oxide belonging to the titanate family. It is the closest compound to $SrTiO_3$ (STO),[1] which was extensively studied over the last decades and is among the standard substrate materials employed for the deposition of oxide thin films. An interesting aspect of ETO is that it is iso-structural to STO, with almost identical lattice constants.[2] This allows us to grow very high quality thin films, having bulk-like characteristics, on top of STO substrates.[3] At room temperature, $EuTiO_3$ has perovskite crystal structures with cubic lattice, and, upon cooling, it undergoes a cubic to tetragonal transition at about 282 K, driven by oxygen octahedra rotation,[4] which is similar to that observed in STO at 105 K.[5] Specific heat and thermal expansion measurements point toward a first-order phase transition, which also affects Young's modulus temperature dependence.[2,6] Thanks to its magnetic cation, ETO is also characterized by an anti-ferromagnetic transition at $T_N = 5.5$ K.[7] Moreover, it is an incipient ferroelectric, and, despite its negative critical temperature of −175 K, which forbids the transition to a ferroelectric state, pieces of evidence of magneto-dielectric coupling made this compound an interesting candidate as a multiferroic material.[8,9]

In recent years, the possibility to realize prototypical micro-electro-mechanical systems from complex oxide thin films has been demonstrated by taking advantage of selective chemical etching of different oxide compounds.[10–14] In order to develop this new scientific and technological direction, it is of great interest to increase the number of viable oxide materials by discussing their fabrication protocols and characterizing their mechanical properties. Contrary to STO, ETO is resistant to HF, enabling selective chemical etching to realize suspended structures having the desired shape.[15]

In this work, we investigate the mechanical properties of $EuTiO_3$ by fabricating micro-mechanical structures from single crystal thin films deposited on top of STO(100). ETO samples are initially characterized in terms of structural, magnetic, and optical properties and then micro-fabricated into suspended double-clamped bridges and cantilevers. The analysis of their mechanical properties allows us to quantify the ETO built-in strain, strain gradient along the in/out-of-plane directions, and Young's modulus. Temperature-dependent measurements of the cantilever's resonance frequency allow us to investigate the ETO anti-ferro-distortive transition by mechanical methods, which was analyzed taking into account contributions from thermal expansion and Young's modulus temperature dependence. At last, we discuss how oxygen vacancies, one of the most common doping defects in complex oxides, affect the reported characteristics.

EXPERIMENTAL

$EuTiO_3$ thin films were grown by pulsed laser deposition on top of $SrTiO_3(100)$ single-crystal substrates kept at 650 °C. We employed a KrF excimer laser (248 nm) with a repetition rate of 4 Hz. The energy density on the target was 1.7 J/cm^2, and the distance between the target and the substrate was 50 mm. The growth chamber base pressure was 1×10^{-6} mbar, and, where not stated differently, the background oxygen pressure during the deposition was 1.5×10^{-4} mbar. Thickness measurements are discussed in the supplementary material Sec. I. Atomic Force Microscope (AFM) imaging has been performed by using a Bruker dimension ICON with a nanoscope 6 controller in tapping mode. Suspended micro-structures were fabricated by UV lithography of SPR-220 photo-resist spin-coated at 6000 RPM for 45 s, followed by baking at 120 °C for 135 s. ETO was removed by dry etching with an Argon milling system having sample water-cooling. Etching time was 45 mins, and Ar ions energy was 500 eV with a current density of 0.2 mA/cm^2. Samples were cleaned from photo-resist residues by room-temperature ultrasonic baths of acetone followed by ethanol and then dried under nitrogen flow. Selective etching of the STO substrate was obtained by soaking the samples in a 5% HF aqueous solution kept at 35 °C in bain-marie for 30 mins. During the bath, the samples were kept suspended above a magnetic stirrer rotating at 200 RPM. They were then transferred to a deionized water bath, followed by two different baths of pure ethanol to remove the presence of water. Finally, they were dried in a CO_2 critical point dryer system. Mechanical characterizations were performed in a custom setup providing PID-controlled temperature and 2×10^{-5} mbar base pressure. When not stated otherwise, the mechanical measurements were performed at a constant temperature of 25 °C. All the mechanical spectra were recorded by measuring the thermal noise of the ETO cantilevers in the optical-lever detection scheme. We employed a 670 nm laser focused on top of the structures with an optical power of 60 μW. The reflected light was converted into an electrical signal by a custom four quadrant photo-diode connected to a spectrum analyzer. The reported spectra were typically the result of eight averages, with a bandwidth depending on the central frequency value starting at 1 Hz when measuring around 13 kHz.

RESULTS

The ETO crystal structure was investigated by x-ray diffraction, and a Θ–2Θ scan of a 100 nm-thick film is reported in Fig. 1(a). ETO peaks cannot be resolved due to the superposition with those owing to the STO substrate, as further confirmed by reciprocal space maps reported in the supplementary material Sec. II. This is in agreement with previous reports of stoichiometric bulk-like ETO films grown in similar conditions.[3] Surface morphology was investigated by atomic force microscopy (AFM), showing a very smooth ETO film surface with a RMS roughness of about 0.1 nm over a scan area of 2.5 × 2.5 μm^2, as shown in Fig. 1(b). This is representative of all the samples analyzed in this work, as reported in the supplementary material Sec. III. Our fabrication protocol is based on standard UV mask lithography, and its main steps are schematically shown in Fig. 1(c), while details are discussed in the experimental section. ETO film is patterned by Ar ion milling and then cleaned in ultrasound acetone and ethanol baths, while selective etching of the STO substrate is obtained by soaking the samples in HF diluted at 5% in water. The etching of STO starts out-of-plane, from the exposed regions, and then proceeds by removing the substrate below the edges of the ETO film, making the narrower geometries suspended.[15] In about 30 mins, all the structures having a width of below 5 μm are completely released and ready for the mechanical characterizations.

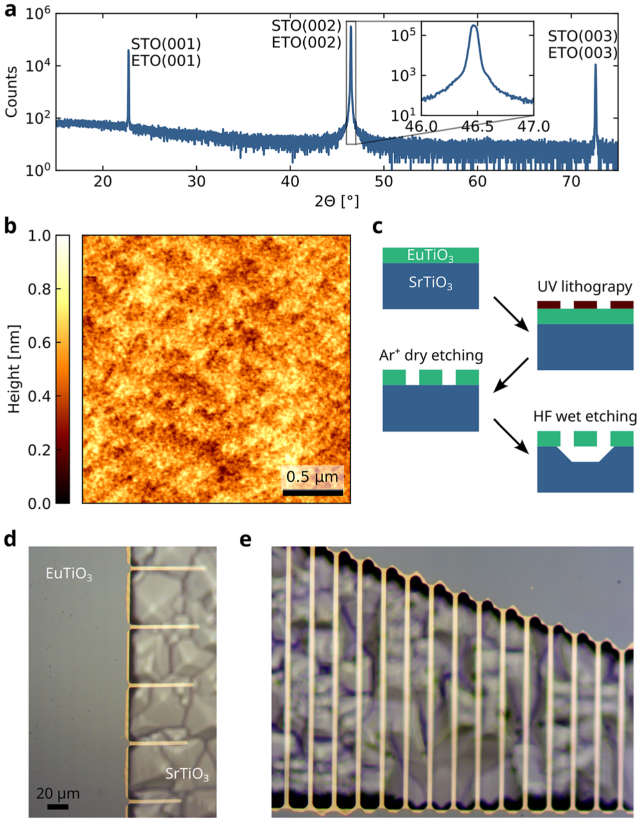

FIG. 1. $EuTiO_3$ film characteristics and device fabrication. (a) XRD scan of a 100 nm-thick ETO film. (00*l*) peaks are superimposed on the ones of the STO(001) substrate. (b) Tapping mode AFM topography image of the ETO surface. (c) Schematic fabrication steps of the ETO suspended structures. (d) and (e) Optical micrographs of ETO cantilevers and micro-bridges.

Examples of the two kinds of geometries employed in this work, cantilevers and double-clamped bridges, are shown in Figs. 1(d) and 1(e), respectively, all having a nominal width of 5 μm. In these pictures, the clamped ETO is dark/blueish, while all the suspended regions are light/yellowish. The typical pyramids that form on top of the STO(100) substrates after HF etching are visible in the background; these are the regions where ETO was removed by ion milling. The nominal length of the cantilevers spans from 15 to 100 μm. In our samples, all the cantilevers up to 60 μm were measurable, while all those above 75 μm were touching the substrate. This relatively sharp threshold is due to the balance between the downward bending of the cantilevers (signaling out-of-plane strain gradient) and the etching depth of the STO substrate, of about 6 μm, making the tip of longer ones to reach the substrate and sticking to that. Touching can be avoided by increasing the wet etching time, but in such a case, liquid flow due to stirring may also become a limiting factor by bending and breaking longer structures. Double-clamped micro-bridges, instead, do not easily collapse and were fabricated with lengths ranging from 100 to 250 μm. As visible in Fig. 1(e), their center is out-of-focus due to the relaxation of built-in compressive strain by buckling.

We can quantitatively evaluate the strain of an ETO film from the shape analysis of buckled double-clamped micro-bridges.[14] To do so, we measured the profile of each bridge by using an optical profilometer, which is an interferometric microscope providing a height map of its field of view. An example of the profiles extracted from these maps is reported in Fig. 2(a), showing an array of ETO micro-bridges having lengths between 100 and 195 μm. Notably, they are all bent downward, which is the most common case in our samples. This could be related to the fabrication process or to strain relaxation at the clamping points. For each individual profile, we calculated the best fit of a sum of trigonometric functions. The resulting analytical expression was then employed to obtain the profile length L^{P}, which was compared to its nominal value L to calculate the strain ε

$$\varepsilon = (L^{\mathrm{P}} - L)/L. \tag{1}$$

This analysis is based on the assumption that all the in-plane compressive stress of the bridge is relaxed and converted into strain (elongation) upon the structure release. The Python script implementing the strain analysis is included in the dataset associated with this work, as indicated in the "Data Availability" section.

In this study, we measured ∼140 micro-bridges fabricated on two different ETO thin film samples having thickness of 97 and 100 nm. The calculated strain distribution of the whole dataset is reported in the histogram of Fig. 2(b), showing an average strain of $\bar{\varepsilon} = +0.14\% \pm 0.02\%$, where the positive sign corresponds to compressive state. The resulting $\bar{\varepsilon}$ implies an in-plane lattice compression of ETO films of $a_{\mathrm{STO}} \cdot \bar{\varepsilon}/(1 + \bar{\varepsilon}) = 0.55$ pm. Under elastic deformation, this would correspond to an expansion of the c-axis in the out-of-plane direction of 0.85 pm, calculated considering a Poisson's ratio of 0.22, as obtained from Ref. 16 (see the supplementary material Sec. IV). Literature reports of ETO pseudo-cubic lattice constants at 300 K indicate values between 3.860 and 3.908 Å.[3,4,16,17] Such dispersion is wider than our calculated lattice deformation due to epitaxial growth, making it difficult to uniquely correlate the in-plane strain to out-of-plane lattice expansion from XRD data reported in Fig. 1. ETO films grown on top of STO are thus likely

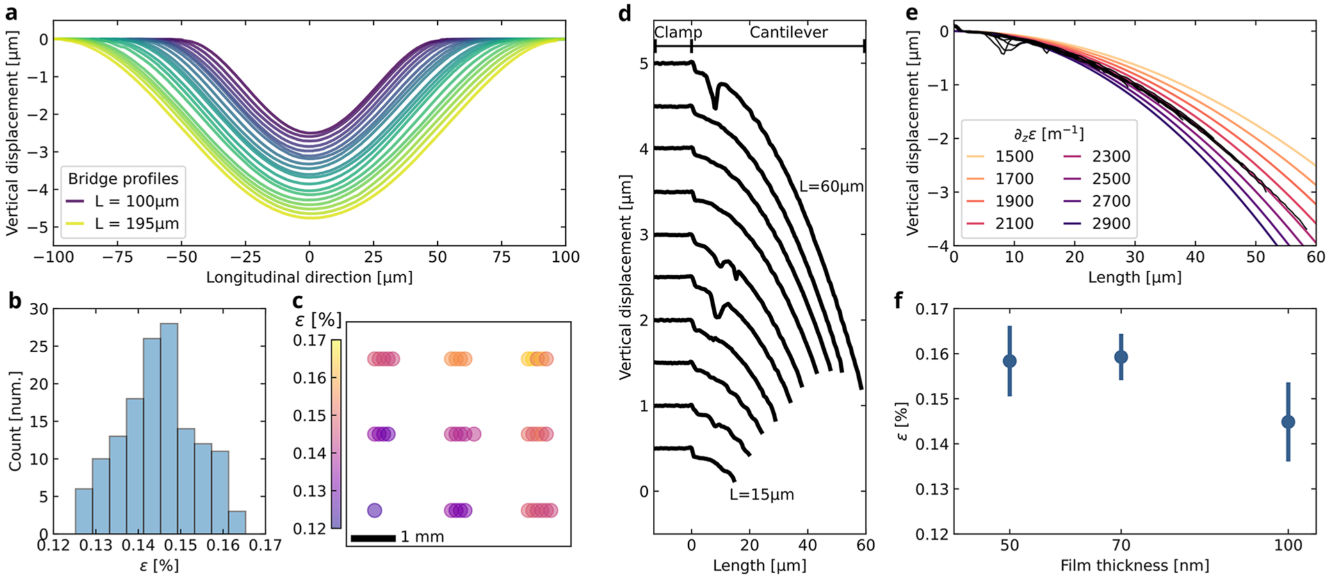

FIG. 2. Strain analysis of $\mathrm{EuTiO_3}$ films. (a) Profiles of ETO double-clamped bridges having different lengths. (b) Histogram of the strain values calculated from a profile length of ∼140 buckled bridges. (c) Strain map of an ETO film, the square represents a 5 × 5 mm^2 substrate where each point is a bridge at its real position. (d) Profiles of cantilevers having different lengths showing the bending due to the out-of-plane strain gradient. The vertical shift is 0.5 μm for better visibility. (e) Comparison between (black) superimposed experimental profiles from (d) and (colors) simulated ones calculated for different strain gradient values. (f) Average strain values obtained for ETO films having different thicknesses, the bars indicate one standard deviation.

at the crossover between tensile and compressive strain, depending on the specific growth condition and crystal defects. Our conclusion is that the measured compressive strain is the result of the formation of thermodynamically stable defects during the growth, such as oxygen vacancies or dislocations.

The width of the strain distribution was found to be related to long-range film inhomogeneities and not to random bridge-to-bridge variations. This is shown in the strain map reported in Fig. 2(c), where the black frame represents the edges of the 5×5 mm^2 STO substrate. Each colored circle is located at the real position of an ETO micro-bridge, and its color indicates the measured strain value. Strain magnitude increases from the bottom-left to the top-right corner, while bridges close to each other show smaller strain values dispersion. Analysis of strain variation of bridges from the same set, such as those belonging to the same harp structure shown in Fig. 2(a), is reported in the supplementary material Sec. V. Similar characteristics were already observed in manganite thin films, likely related to temperature gradients or to small variations in film stoichiometry due to substrate-plume misalignment during the growth.[18]

While double-clamped bridges provide information about in-plane strain, cantilevers do not, because, thanks to their free end, stress is relaxed by elongating the structures and not by buckling. However, cantilevers can be employed to evaluate the strain gradient in the out-of-plane direction $(\partial_z \varepsilon_{x,y})$, because it results in vertical bending of the structures due to the different in-plane strain between top and bottom surfaces. Figure 2(d) shows a set of profiles owing to cantilevers having lengths between 15 and 60 μm. Here, the horizontal coordinate was shifted to align at $x = 0$ at the beginning of the suspended regions, while all the profiles were vertically shifted by 0.5 μm for better visibility. The irregularities in the profiles are artifacts of the measurement technique, which fails to reconstruct the shape of these semi-transparent structures where the substrate is close below. All the cantilevers are bent downward, signaling a positive strain gradient in the vertical direction. Such gradients can be quantitatively evaluated by comparing the measured profiles with what is expected from a simple finite element model based on a constant vertical gradient, which is reported in Fig. 2(e). Here, the black lines are all the measured profiles of 2d collapsed on top of each other, while the colored lines are profiles calculated for different values of $\partial_z \varepsilon$. The best agreement is found for $\partial_z \varepsilon = 2300$ m^{-1}, with a confidence interval of about 5%, i.e., one-half of the 200 m^{-1} line spacing. Since the ETO thickness is $t = 97$ nm, the resulting in-plane strain difference between the bottom and top surfaces is $\Delta\varepsilon = \partial \varepsilon_z \times t = 0.023\%$, which is about six times smaller than the average in-plane strain.

To further understand the characteristics of strain and strain relaxation in ETO thin films, we grew films having different thicknesses and measured their average in-plane strain from the profile analysis of buckled micro-bridges. Apparently, thinner films have a slightly higher compressive strain, as shown in Fig. 2(f). From this comparison, we conclude that strain relaxation does not evolve layer-by-layer during the growth; otherwise, we would observe an increase in strain value for thicker structures due to the positive gradient. It is instead a global characteristic of the crystal that likely evolves across its whole thickness as long as the growth process continues, at least for the explored film thickness range.

Even if slightly bent out-of-plane, micro-cantilevers can be employed as mechanical resonators to obtain the Young's modulus of the ETO film.[19] The resonance frequency can be calculated by using Euler–Bernoulli theory assuming a linear elastic material and small deflections. The resonance frequency of the flexural modes (f_n) of our cantilevers is modeled assuming thin and long beams having width much greater than their thickness (plate approximation).[20]

$$f_n = \frac{\lambda_n^2}{2\pi} \frac{t}{L^2} \sqrt{\frac{E}{12\rho(1-\nu^2)}}, \tag{2}$$

where $\lambda_n = \{1.8751,\ 4.6941,\ 7.8548,\ (2n-1)\pi/2\}$ is a numerical parameter related to the mode shape, t is the thickness, L the length, ρ the density, and E the Young's modulus. We note that Eq. (2) has no stress dependence. This is because, as previously discussed, in cantilevers, the longitudinal stress is relaxed due to their free ends. To confirm that the simple analytical model of Eq. (2) can be applied to our ETO resonators, we first measured a wide spectrum of a 75 μm-long cantilever, which is reported in Fig. 3(a). The first flexural mode is located at 12.7 kHz, the second at 79.6 kHz, and the third at 224.2 kHz. Since the mode spacing should only be given by the numerical factors λ_n in Eq. (2), we can take the first mode as a reference and calculate the expected values of the higher modes as $f_n = f_1 \lambda_n / \lambda_1$. The resulting frequencies are marked by the green bands in Fig. 3(a) and well-match the experimental values. Figure 3(b) shows a detailed spectrum of the first flexural mode, where the black line is a fit

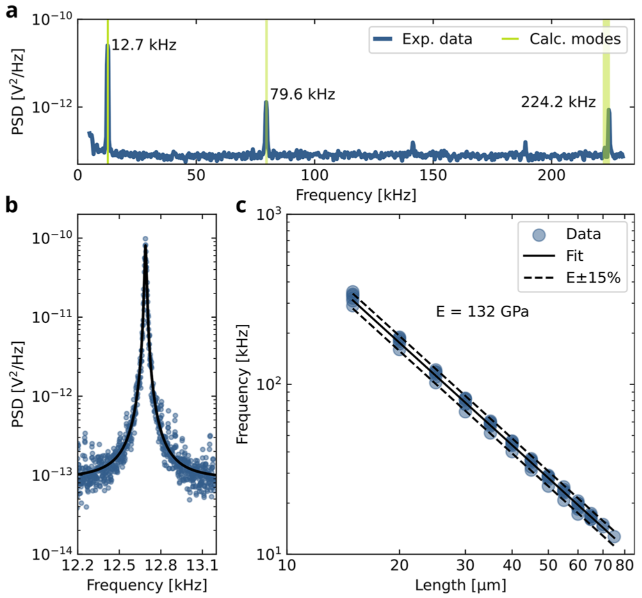

FIG. 3. $EuTiO_3$ cantilever resonators. (a) Spectrum of a 75 μm-long cantilever. Green lines indicate the expected position of the flexural modes from Eq. (2) by rescaling the frequency of the first one. Linewidth indicates uncertainty. (b) Thermal noise spectrum of the first flexural mode of a 75 μm-long ETO cantilever. (c) Frequency vs length for ETO cantilevers (blue dots); Young's modulus was obtained from fitting Eq. (2) (black solid line). All the data points lie in a ±15% range (black dashed lines) around the best fit value for *E*.

of the analytical expression of the thermal noise spectrum.[21] The resulting Q factor of 960 is in line with the other ETO cantilever resonators fabricated on these samples, all between 600 and 1300. These values are much lower than what was recently reported for other complex oxide micro-bridge resonators, exceeding 10k,[18] this because double-clamped geometries under tension may take advantage of dissipation–dilution mechanism to enhance their Q factor.[22]

We measured several ETO cantilevers having lengths spanning from 15 to 75 μm and reported their first eigenfrequency f_1 in the scatter plot of Fig. 3(c). In order to calculate the ETO Young's modulus (E_{ETO}) from this dataset, we fit Eq. (2) considering a theoretical density of 6916.5 kg/m^3, calculated from the Eu, Ti, and O atomic masses, and a (3.9 Å)^3 cubic unit cell volume. To evaluate the dispersion of the measured resonance frequencies around their best fit (black solid line), in Fig. 3(c), we mark the E_{ETO} ±15% window (dashed black lines) comprising all the data points. The resulting E_{ETO} = 132 GPa is about one-half of what was obtained from measurements of resonant ultrasound spectroscopy in bulk single crystal samples, where the reported elastic moduli correspond to a Young's modulus of about 280 GPa (see the supplementary material Sec. V).[16] However, this result is in line with a recent study about the mechanics of ultra-thin SrTiO$_3$, which shows that a Young's modulus of 100 nm-thick STO membranes is just below one-half of the bulk value.[23]

By measuring the temperature dependence of the resonance frequency of ETO cantilever resonators, it is also possible to investigate the EuTiO$_3$ anti-ferro-distortive transition characteristics. To do so, we measured a 20 μm-long cantilever that was initially cooled down from room temperature to 255 K. The thermal noise spectrum of its first flexural mode was then recorded every 0.5 K during both heating and cooling stepped ramps. The eigenfrequency vs temperature characteristics ($f_1(T)$) are reported in Fig. 4(a), showing two distinct features: (i) a slope change during heating between 275 and 295 K and (ii) a thermal hysteresis. We can separate the contributions from thermal expansion and Young's modulus temperature dependence by considering the relative temperature derivative of the squared frequency

$$\frac{\partial_T f_1^2}{f_1^2} = \alpha(T) + \frac{\partial_T E}{E}, \tag{3}$$

where $\alpha(T)$ is the linear expansion coefficient. Equation (3) was obtained from Eq. (2) as discussed in the supplementary material, Sec. VI. In Fig. 4(b), we compare the experimental $\partial_T f_1^2/f_1^2$ (solid lines) with the thermal expansion coefficient as exacted from Ref. 6 (dashed line). Thermal expansion is small if compared to the experimental measurements, peaking at 35 ppm/K at 282 K and flattening out at about 15 ppm/K at high temperatures. As a consequence, Young's modulus provides the dominant contribution to the measured slope, with a high-temperature constant value of about −200 ppm/K. From the $f_1(T)$ data, we can also obtain the Young's modulus of ETO by considering the first-order thermal expansion approximation for t, L, and ρ in Eq. (2).

$$E(T) = E_{T_0} \frac{f_1^2}{f_{1,T_0}^2} \frac{1}{(1 + A(T))}, \tag{4}$$

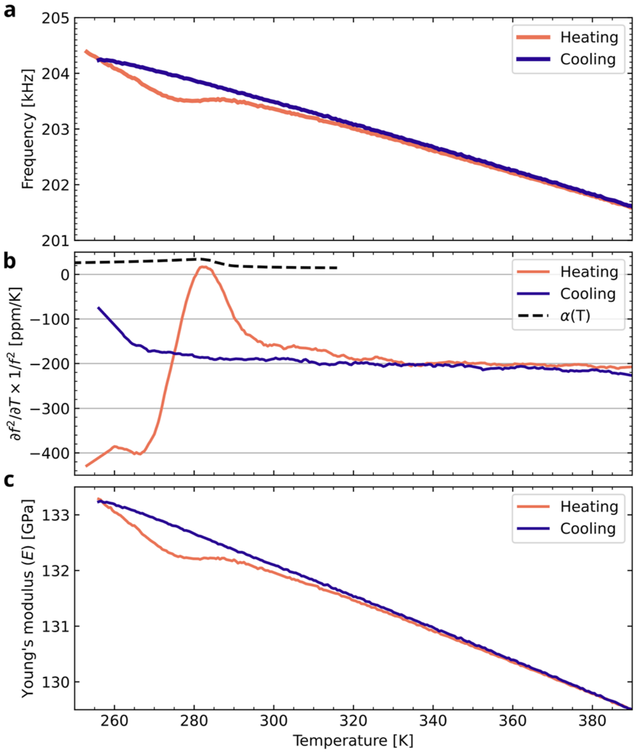

FIG. 4. Anti-ferro-distortive transition of EuTiO$_3$ detected by resonance frequency measurements. (a) Frequency vs temperature characteristics of the first flexural mode of a 20 μm-long cantilever during heating and cooling ramps. (b) Relative temperature derivative of the squared frequency data from (a). Black dashed line is thermal expansion appearing in Eq. (3), as extracted from Ref. 2. (c) Temperature dependence of the ETO Young's modulus obtained from cantilever eigenfrequency measurements.

where T_0 is the reference temperature of 298 K at which we measured the Young's modulus of 132 GPa [see Fig. 3(c)] and $A(T)$ is the integral function of the thermal expansion $\alpha(T)$ calculated between T_0 and T, as discussed in the supplementary material, Sec. VI.

The anomaly of Young's modulus, marked by the oscillatory behavior of $\partial_T f_1^2/f_1^2$ below 300 K, indicates the onset of the anti-ferro-distortive transition. This is in agreement with a previous report from Schiemer *et al.*,[24] showing large variations of the stiffness moduli in the proximity of the transition temperature in both single crystal and polycrystalline bulk ETO samples measured by resonant ultrasound spectroscopy. A key difference between our results and those of these previous studies is the width of the thermal hysteresis, which in their experiment was about 1 K. In our case, instead, thermal hysteresis is about 35 K, as estimated in Fig. 4(b). This wider transition could be due to the high surface/volume ratio of our thin film-based devices, since hysteresis widening driven by size effects has already been reported for other materials showing first order phase transition.[25,26] Another possible contribution is the presence of thermal gradients along the cantilever, since the clamping point is in better contact with the thermal bath and the tip dissipates more. However, considering a background pressure of 2×10^{-5} mbar, such an effect is expected to be small. Because of the limited temperature span of our measurement setup, we could not access the whole hysteresis width. Such hysteretic behavior was observed in several devices fabricated on different samples, as reported in the supplementary material, Sec. VII, where differences in hysteresis width and amplitude are related to the nature of nested loops, whose shape is critically dependent on the extremal temperatures. Detailed analysis of this behavior will require dedicated experiments involving a wider temperature range, samples having different thicknesses and cantilever geometries, and, ideally, a magnetic field.

Finally, we investigated how the $EuTiO_3$ characteristics reported so far are affected by oxygen vacancies, which are a typical defect, as well as the doping mechanism of complex oxides. To do so, we grew nominally 100 nm-thick films at a lower oxygen pressure of 10^{-6} mbar instead of 10^{-4} mbar. Its actual thickness, however, was 83 nm, as reported in the supplementary material, Sec. I. After the preliminary characterizations reported in Figs. 5(a)–5(c), $ETO_{3-\delta}$ samples underwent the same fabrication protocol as stoichiometric ones. The formation of oxygen vacancies is indicated by the XPS data reported in Fig. 5(a), where the valence change of Eu atoms with added weight on Eu^{2+}, is a consequence of charge balance after oxygen removal. Another feature of $ETO_{3-\delta}$ films is the onset of a ferro-magnetic transition at low temperature, as evidenced by an inflection point in the $\chi(T)$ characteristic.[3] This feature is visible in our SQUID data as evidenced by the black arrow in Fig. 5(b). XRD measurements reported in Fig. 5(c) show that oxygen-deficient samples have a larger out-of-plane inter-planar distance. Such lattice expansion is a common feature of oxygen vacancies-doped complex oxides,[27,28] which is associated with an increase in the compressive strain of the material. Moreover, the broadening of the diffraction peak is quite large, also showing peak splitting.

A peculiar characteristic of $ETO_{3-\delta}$ samples is strain inhomogeneity, as exemplified by the strain map in Fig. 5(e), which shows strong variations between the upper and lower edges. Similar strain gradients were observed across four samples grown in different deposition runs and were always associated with broad XRD peaks, similar to what is reported in Fig. 5(c). Because of that, we hypothesize that oxygen deficiency during growth makes ETO much more sensitive to small temperature gradients or substrate inhomogeneities, which, in higher pressure conditions, do not affect long-range strain characteristics. Another dramatic difference between stoichiometric and vacancy-doped cases is the out-of-plane strain gradient. Figure 5(f) compares the profiles of two 40 μm-long cantilevers: the $ETO_{3-\delta}$ one is bent upward and shows a much larger displacement than the stoichiometric case. The strain gradient is thus negative and about three times larger. This feature is quite surprising, because in a simple layer-by-layer growth picture, we could expect better film oxidation at the bottom layers due to oxygen exchange with the STO substrate. However, in such a case, the bottom surface of the cantilever would be more compressed, resulting in a profile shape similar to the ETO_3 case. This result supports our previous conclusion that strain and strain gradients behave as global film characteristics determined during the entire deposition process. We also investigate whether the Young's modulus of $ETO_{3-\delta}$ was affected by oxygen vacancies by analyzing the frequency vs length relationship of an array of cantilevers, as in Fig. 3(c). As reported in Fig. 5(f), this is not the case because the difference between the resulting Young's moduli, of just 2 GPa, is within the experimental error, while the lower resonance frequencies for the $ETO_{3-\delta}$ cantilevers are due to the thickness of the films (t_{ETO_3} = 97 nm and $t_{ETO_{3-\delta}}$ = 83 nm).

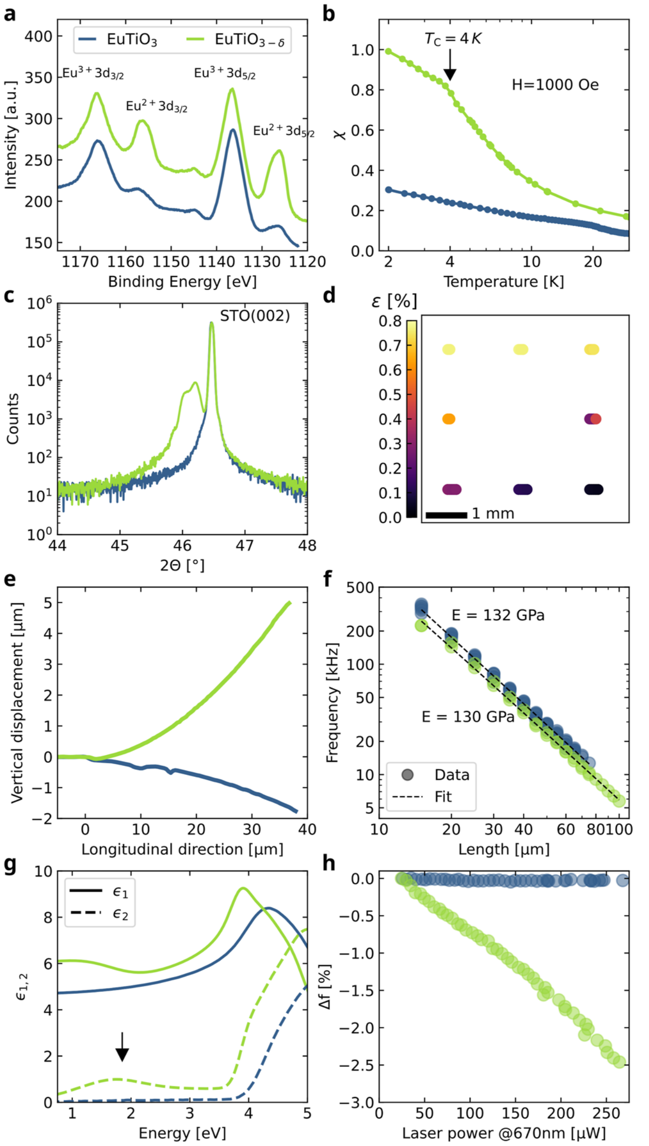

FIG. 5. Comparison between $EuTiO_3$ (blue) and $EuTiO_{3-\delta}$ (green). (a) XPS spectra of the different Eu oxidation states. (b) SQUID measurement showing paramagnetic response and ferro-magnetic transition (arrow) $ETO_{3-\delta}$. (c) XRD around the (002) peak of the STO substrate. (d) Strain map of an $ETO_{3-\delta}$ sample calculated as in Fig. 2(c). (e) Profiles of 40 μm cantilevers signaling opposite out-of-plane strain gradients. (f) Young's modulus obtained from the resonance frequency of ETO cantilevers. Data of stoichiometric sample are from Fig. 3(c). (g) Dielectric constants of ETO thin films. The black arrow marks the wavelength of the laser employed in (h). (h) Frequency shift vs optical power measured on two 65 μm-long cantilevers.

It is well known that the formation of oxygen vacancies affects the light absorption of complex oxides.[29] To understand how this happens in ETO$_{3-\delta}$, we assessed the optical properties of stoichiometric and oxygen-deficient films, prior to microfabrication, by means of spectroscopic ellipsometry. The complex dielectric functions ϵ of the substrate and the ETO film were modeled as a superposition of PSEMI oscillators (parameterized functions used to describe the optical response of crystalline semiconductors).[30,31] The values of ϵ extracted from the ellipsometry data, reported in Fig. 5(g), indicate that stoichiometric samples show no absorption below the band-gap, located at about 4 eV, in agreement with previous reports.[32] Oxygen vacancies determine a small red-shifting of the bandgap, from 4.0 to 3.6 eV, but critically increase ϵ_2 (green dashed line) in the low-energy region, signaling the formation of in-gap states leading to broadband light absorption. An increased optical absorption affects the response of mechanical resonators to incident light. We thus compared the resonance frequency shift of two 65 μm-long cantilevers, one made of ETO$_3$ and the other from ETO$_{3-\delta}$ as a function of the incident light power. The laser is the same employed to probe the motion of the structure, and its wavelength of 670 nm corresponds to the arrow in Fig. 5(g). The resulting tuning slopes are reported in Fig. 5(h), where, for better comparison, we considered the relative frequency shift with respect to the lowest power employed in the experiment (25 μW). The stoichiometric sample shows almost no softening and thus no heating, in agreement with its good transparency. ETO$_{3-\delta}$ cantilever, instead, lowers its eigenfrequency to about 2.5% for an incident light power of $P = 250\ \mu$W. This can be compared to the frequency shift measured during the temperature ramps in Fig. 4(b) by considering the finite differences

$$\frac{\Delta f^2}{\Delta P}\frac{1}{f_0^2} = \frac{(1.025 f_0)^2 - f_0^2}{f_0^2 \Delta P} = \frac{0.05}{\Delta P} = 200\left[\frac{\text{ppm}}{\mu\,\text{W}}\right]. \qquad (5)$$

Quite nicely, we found a 1 μW ↔ 1 K equivalence, which holds for this specific cantilever length and above 300 K.

CONCLUSIONS

In summary, we investigated the mechanical properties of stoichiometric and oxygen vacancy-doped EuTiO$_3$ by fabricating suspended micro-structures from single-crystal thin films grown on top of SrTiO$_3$(001) substrates. Mechanical characterization measurements provided a quantitative evaluation of average in/out-of-plane strain and strain gradients as well as the Young's modulus of the material. Stoichiometric films are found slightly compressed, with an average strain of +0.14%, while oxygen-deficient ones show higher strain inhomogeneity. The Young's modulus of about 132 GPa is almost one-half of what is found in bulk samples, in line with recent measurements on SrTiO$_3$ membranes having similar thickness. Temperature-dependent mechanical measurements indicate that above 300 K, the relative derivative of the Young's modulus is about −200 ppm/K. Below 300 K, we observe a non-monotonic and hysteretic mechanical response associated with the EuTiO$_3$ antiferro-distortive transition. Its width of about 35 K is a striking difference with respect to bulk samples that show a small hysteresis of about 1 K. Such widening could be related to size effects or temperature gradients across the structure, but a clear understanding of its origin will require new dedicated experiments.

SUPPLEMENTARY MATERIAL

The supplementary material of this article contains EuTiO$_3$ growth data and thickness calibration, reciprocal space maps of stoichiometric and oxygen-deficient samples, surface topography of as-grown EuTiO$_3$ thin films, evaluation of bulk EuTiO$_3$ Young's modulus and Poisson's ratio from literature data, analysis of strain variations within bridges owing to the same harp array, derivation of Eqs. (3) and (4), and frequency vs temperature data, as those reported in Fig. 4(a), measured on different cantilevers.

ACKNOWLEDGMENTS

We thank Emilio Bellingeri, Gianrico Lamura, Cristina Bernini, and Alejandro Enrique Plaza for useful discussions. This work was carried out under the OXiNEMS project (www.oxinems.eu). This project has received funding from the European Union's Horizon 2020 research and innovation program under Grant Agreement No. 828784. We acknowledge financial support from the Università di Genova through the "Fondi di Ricerca di Ateneo" (FRA). We also acknowledge support from the Swedish infrastructure for micro- and nano-fabrication–MyFab.

AUTHOR DECLARATIONS

Conflict of Interest

The authors have no conflicts to disclose.

Author Contributions

Nicola Manca: Conceptualization (lead); Data curation (lead); Formal analysis (equal); Investigation (lead); Resources (equal); Supervision (equal); Visualization (lead); Writing – original draft (lead); Writing – review & editing (equal). **Gaia Tarsi**: Formal analysis (equal); Investigation (equal); Writing – review & editing (equal). **Alexei Kalaboukhov**: Data curation (equal); Formal analysis (supporting); Investigation (equal); Resources (equal); Writing – review & editing (supporting). **Francesco Bisio**: Data curation (equal); Formal analysis (supporting); Investigation (supporting); Writing – review & editing (equal). **Federico Caglieris**: Data curation (equal); Formal analysis (supporting); Investigation (supporting); Writing – review & editing (supporting). **Floriana Lombardi**: Funding acquisition (equal); Project administration (equal); Writing – review & editing (equal). **Daniele Marré**: Conceptualization (equal); Funding acquisition (equal); Project administration (equal); Supervision (equal); Writing – review & editing (equal). **Luca Pellegrino**: Conceptualization (equal); Funding acquisition (lead); Investigation (equal); Project administration (lead); Resources (supporting); Supervision (equal); Writing – review & editing (equal).

DATA AVAILABILITY

The numerical data shown in the figures of this manuscript and the supplementary material can be downloaded from the Zenodo online repository: http://dx.doi.org/10.5281/zenodo.8109185.

REFERENCES

[1] A. Bussmann-Holder, J. Köhler, R. K. Kremer, and J. M. Law, "Relation between structural instabilities in $EuTiO_3$ and $SrTiO_3$," Phys. Rev. B **83**, 212102 (2011).

[2] V. Goian, S. Kamba, O. Pacherová, J. Drahokoupil, L. Palatinus, M. Dušek, J. Rohlíček, M. Savinov, F. Laufek, W. Schranz, A. Fuith, M. Kachlík, K. Maca, A. Shkabko, L. Sagarna, A. Weidenkaff, and A. A. Belik, "Antiferrodistortive phase transition in $EuTiO_3$," Phys. Rev. B **86**, 054112 (2012).

[3] K. Fujita, N. Wakasugi, S. Murai, Y. Zong, and K. Tanaka, "High-quality antiferromagnetic $EuTiO_3$ epitaxial thin films on $SrTiO_3$ prepared by pulsed laser deposition and postannealing," Appl. Phys. Lett. **94**, 062512 (2009).

[4] J. Köhler, R. Dinnebier, and A. Bussmann-Holder, "Structural instability of $EuTiO_3$ from x-ray powder diffraction," Phase Transitions **85**, 949–955 (2012).

[5] G. Shirane and Y. Yamada, "Lattice-dynamical study of the 110 K phase transition in $SrTiO_3$," Phys. Rev. **177**, 858–863 (1969).

[6] P. G. Reuvekamp, R. K. Kremer, J. Köhler, and A. Bussmann-Holder, "Evidence for the first-order nature of the structural instability in $EuTiO_3$ from thermal expansion measurements," Phys. Rev. B **90**, 104105 (2014).

[7] T. R. McGuire, M. W. Shafer, R. J. Joenk, H. A. Alperin, and S. J. Pickart, "Magnetic structure of $EuTiO_3$," J. Appl. Phys. **37**, 981–982 (1966).

[8] T. Katsufuji and H. Takagi, "Coupling between magnetism and dielectric properties in quantum paraelectric $EuTiO_3$," Phys. Rev. B **64**, 054415 (2001).

[9] A. Bussmann-Holder and J. Köhler, "Revisiting the fascinating properties of $EuTiO_3$ and its mixed crystals with $SrTiO_3$: Possible candidates for novel functionalities," J. Phys. Chem. Solids **84**, 2–12 (2015).

[10] L. Pellegrino, M. Biasotti, E. Bellingeri, C. Bernini, A. S. Siri, and D. Marré, "All-oxide crystalline microelectromechanical systems: Bending the functionalities of transition-metal oxide thin films," Adv. Mater. **21**, 2377–2381 (2009).

[11] N. Manca, L. Pellegrino, T. Kanki, W. J. Venstra, G. Mattoni, Y. Higuchi, H. Tanaka, A. D. Caviglia, and D. Marré, "Selective high-frequency mechanical actuation driven by the VO_2 electronic instability," Adv. Mater. **29**, 1701618 (2017).

[12] N. Manca, G. Mattoni, M. Pelassa, W. J. Venstra, H. S. J. van der Zant, and A. D. Caviglia, "Large tunability of strain in WO_3 single-crystal microresonators controlled by exposure to H_2 gas," ACS Appl. Mater. Interfaces **11**, 44438–44443 (2019).

[13] N. Manca, T. Kanki, F. Endo, D. Marré, and L. Pellegrino, "Planar nanoactuators based on VO_2 phase transition," Nano Lett. **20**, 7251–7256 (2020).

[14] N. Manca, T. Kanki, F. Endo, E. Ragucci, L. Pellegrino, and D. Marré, "Anisotropic temperature-driven strain dynamics in VO_2 solid-state microactuators," ACS Appl. Electron. Mater. **3**, 211–218 (2021).

[15] A. E. Plaza, N. Manca, C. Bernini, D. Marré, and L. Pellegrino, "The role of etching anisotropy in the fabrication of freestanding oxide microstructures on $SrTiO_3(100)$, $SrTiO_3(110)$, and $SrTiO_3(111)$ substrates," Appl. Phys. Lett. **119**, 033504 (2021).

[16] L. Li, J. R. Morris, M. R. Koehler, Z. Dun, H. Zhou, J. Yan, D. Mandrus, and V. Keppens, "Structural and magnetic phase transitions in $EuTi_{1-x}Nb_xO_3$," Phys. Rev. B **92**, 024109 (2015).

[17] P. Pappas, A. Bussmann-Holder, H. Keller, E. Liarokapis, and K. Roleder, "Complex symmetry of phases and magnetic properties of $EuTiO_3$," Phys. Rev. B **106**, 214306 (2022).

[18] N. Manca, F. Remaggi, A. E. Plaza, L. Varbaro, C. Bernini, L. Pellegrino, and D. Marré, "Stress analysis and Q-factor of free-standing (La, Sr)MnO_3 oxide resonators," Small **18**, 2202768 (2022).

[19] L. Kiesewetter, J.-M. Zhang, D. Houdeau, and A. Steckenborn, "Determination of Young's moduli of micromechanical thin films using the resonance method," Sens. Actuators, A **35**, 153–159 (1992).

[20] S. Schmid, L. G. Villanueva, and M. L. Roukes, *Fundamentals of Nanomechanical Resonators* (Springer International Publishing, Cham, 2016).

[21] B. Hauer, C. Doolin, K. Beach, and J. Davis, "A general procedure for thermomechanical calibration of nano/micro-mechanical resonators," Ann. Phys. **339**, 181–207 (2013).

[22] L. Sementilli, E. Romero, and W. P. Bowen, "Nanomechanical dissipation and strain engineering," Adv. Funct. Mater. **32**, 2105247 (2022).

[23] V. Harbola, S. Crossley, S. S. Hong, D. Lu, Y. A. Birkhölzer, Y. Hikita, and H. Y. Hwang, "Strain gradient elasticity in $SrTiO_3$ membranes: Bending versus stretching," Nano Lett. **21**, 2470–2475 (2021).

[24] J. Schiemer, L. J. Spalek, S. S. Saxena, C. Panagopoulos, T. Katsufuji, A. Bussmann-Holder, J. Köhler, and M. A. Carpenter, "Magnetic field and *in situ* stress dependence of elastic behavior in $EuTiO_3$ from resonant ultrasound spectroscopy," Phys. Rev. B **93**, 054108 (2016).

[25] D. Brassard, S. Fourmaux, M. Jean-Jacques, J. C. Kieffer, and M. A. El Khakani, "Grain size effect on the semiconductor–metal phase transition characteristics of magnetron-sputtered VO_2 thin films," Appl. Phys. Lett. **87**, 051910 (2005).

[26] M. Nazari, Y. Zhao, V. Hallum, A. A. Bernussi, Z. Y. Fan, and M. Holtz, "Finite size effect on the phase transition of vanadium dioxide," Appl. Phys. Lett. **103**, 043108 (2013).

[27] W. S. Choi, Z. Marton, S. Y. Jang, S. J. Moon, B. C. Jeon, J. H. Shin, S. S. A. Seo, T. W. Noh, K. Myung-Whun, H. N. Lee, and Y. S. Lee, "Effects of oxygen-reducing atmosphere annealing on $LaMnO_3$ epitaxial thin films," J. Phys. D: Appl. Phys. **42**, 165401 (2009).

[28] G. Mattoni, A. Filippetti, N. Manca, P. Zubko, and A. D. Caviglia, "Charge doping and large lattice expansion in oxygen-deficient heteroepitaxial WO_3," Phys. Rev. Mater. **2**, 053402 (2018).

[29] J. Blanc and D. L. Staebler, "Electrocoloration in $SrTiO_3$: Vacancy drift and oxidation–reduction of transition metals," Phys. Rev. B **4**, 3548–3557 (1971).

[30] B. Johs, C. Herzinger, J. Dinan, A. Cornfeld, and J. Benson, "Development of a parametric optical constant model for $Hg_{1-x}Cd_xTe$ for control of composition by spectroscopic ellipsometry during MBE growth," Thin Solid Films **313–314**, 137–142 (1998).

[31] M. Sygletou, S. Benedetti, A. di Bona, M. Canepa, F. Bisio, and E. Bellingeri, "In-operando optical spectroscopy of field-effect-gated Al-doped ZnO," ACS Appl. Mater. Interfaces **15**, 3112 (2023).

[32] B. Stuhlhofer, G. Logvenov, M. Górny, K. Roleder, A. Boris, D. Pröpper, R. K. Kremer, J. Köhler, and A. Bussmann-Holder, "New features from transparent thin films of $EuTiO_3$," Phase Transitions **89**, 731–739 (2016).